


SURVEY

Open Access



# A survey on filtered-x least mean square-based active noise control systems with emphasis on reducing computational complexity

Xiaolong Li<sup>1,2</sup>, Wan Chen<sup>1,2\*</sup> , Zhien Liu<sup>1,2</sup>, Chihua Lu<sup>1,2</sup> and Menglei Sun<sup>3</sup>

\*Correspondence:  
wch@whut.edu.cn

<sup>1</sup> Hubei Key Laboratory of Advanced Technology for Automotive Components, Wuhan University of Technology, Wuhan 430070, China

<sup>2</sup> Foshan Xianhu Laboratory of the Advanced Energy Science and Technology Guangdong Laboratory, Foshan 528200, China

<sup>3</sup> Dongfeng Motor Corporation Technical Center, Wuhan 430058, China

## Abstract

Active noise control (ANC) is gaining ever-increasing attention owing to its powerful ability to attenuate low-frequency noise. The computational complexity of an ANC system may directly affect its computational efficiency, control performance, and hardware costs. Therefore, the focus of this paper is mainly on discussing the development of ANC systems with emphasis on reducing computational complexity. The ANC systems are classified into two groups of narrowband and broadband systems. The computational complexity analysis is provided to show the computational merit of each system with respect to the conventional ANC systems. In addition, numerical simulations are performed to evaluate the convergence speed and noise reduction performance of the considered systems. The results show that, in the narrowband ANC systems, the LFE-NANC, CFX-NANC and BFX-NANC systems enjoy better overall performance in terms of the computational complexity, convergence speed and steady-state error, and in the broadband ANC systems, the DF-BANC system has the lowest computational complexity but cannot effectively attenuate the broadband noise with high spectral dynamics, whereas the DS-BANC and MDS-BANC systems can. This study provides in-depth insight into current typical low-complexity ANC systems.

**Keywords:** Active noise control, Computational complexity, FXLMS algorithm, Narrowband ANC systems, Broadband ANC systems

## 1 Introduction

In 1936, Lueg [1] first put forward active noise control (ANC) technique based on the principle of sound wave interference. This technique introduces a controllable secondary source to generate a secondary sound with the same amplitude but opposite phase to cancel the primary noise. Compared to passive noise control (PNC) technique, ANC technique possesses the advantages of exceptional low-frequency control effect, flexible parameter setting and easy implement. Furthermore, the considerable advancement of large-scale integrated circuits and digital signal processing has facilitated ANC

technique a wide range of noise control applications, such as vehicle noise control [2–4], vessel noise control [5–7], and airplane noise control [8–10], etc.

According to the spectral characteristics of primary noise, ANC systems can be divided into narrowband and broadband ANC systems [11, 12]. Currently, the parallel-form narrowband ANC systems are more popular than the direct-form ones, and they usually connect multiple two-weight adaptive notch filters in parallel to control multi-tonal noise [13–15]. Figure 1 shows the block diagram of the conventional filtered-x least mean square (FXLMS) algorithm-based narrowband ANC (FX-NANC) system. In each frequency channel of this system, a synthesized cosine wave and a synthesized sine wave are used as the reference signals, and their amplitudes and phases are adaptively modulated by the adaptive notch filter to track the primary noise. The frequency information used to synthesize the cosine and sine waves is usually given directly or calculated from other signals such as rotating speed signal. According to the principle of FXLMS algorithm, the reference signal needs to be filtered with the estimate of the secondary path to obtain the filtered reference signal for weight updating. Therefore, in each frequency channel, two reference-filtering operations are required for the cosine and sine reference signals. Each reference-filtering operation is actually a convolution operation in the mathematical sense, and the number of multiplications and additions involved depends on the length of the estimated secondary path. This means that when the number of the controlled tonal components and/or the length of the estimated secondary path increases, the computational burden of this system in terms of reference filtering will severely limit its real-world applications.

As for broadband ANC systems, the conventional broadband ANC system is also based on the FXLMS algorithm (the system is called FX-BANC system), as shown in Fig. 2. Different from the FX-NANC system, the FX-BANC system uses a high-order transverse finite impulse response (FIR) filter as the control filter. At each sample point, the system needs to generate the control signal for secondary output and the filtered reference signal for weight updating. Therefore, when the length of the control filter and/or the length of the estimated secondary path is large, the computational load regarding convolution operations of the FX-BANC system will be much more than the FXLMS recursion requirements.

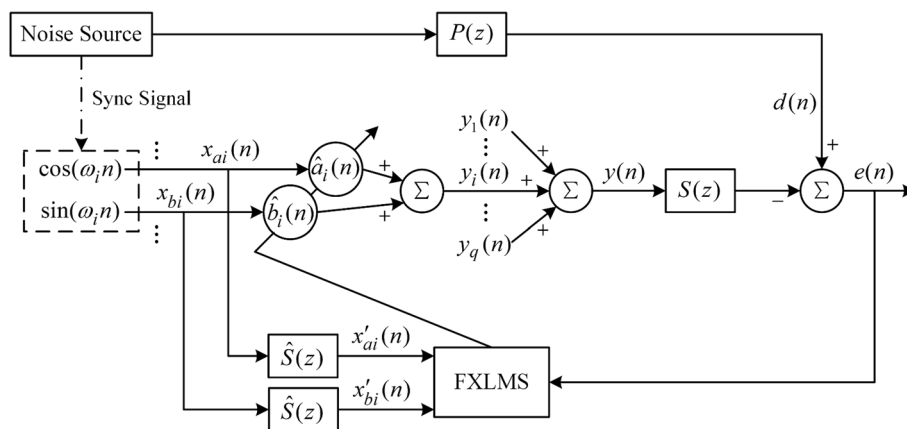
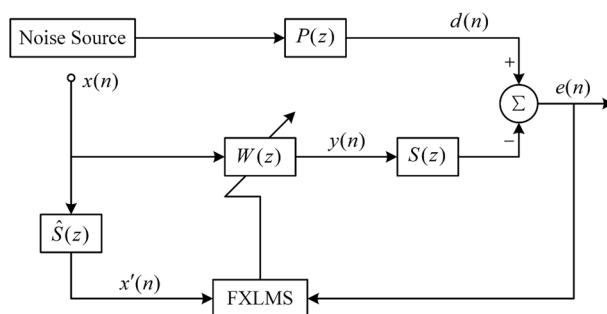


Fig. 1 Block diagram of the conventional FX-NANC system (*i*th channel)



**Fig. 2** Block diagram of the conventional FX-BANC system

Over the past few decades, ANC research has made significant progress in critical performance improvements, including accelerating convergence speed, enhancing robustness and reducing computational complexity. The main approaches to improve the convergence speed of the conventional ANC systems include adaptive variable step size method [16–18], variable tap-length method [19–21] and eigenvalue equalization method [22]. The robustness enhancement approaches for impulse noise are mainly threshold setting method [23, 24], logarithmic transformation method [25] and fractional moment method [23, 26].

A low-computational ANC system can ensure fast computational efficiency to meet the demands of high sampling rate, which is very beneficial especially when tracking time-varying non-stationary noise. Besides, according to Shannon sampling theory, a high sampling rate is also necessary when the controlled noise is a broadband noise such as vehicle interior noise at high speeds. On the other hand, the low computational effort of an ANC system means that it will consume fewer hardware resources, so one may use cheaper hardware available in the market or possibly include the entire ANC system in the controller already installed on the machine. This way, the ANC technique will become more applicable to real machines and products, and can meet the stringent cost requirements of machinery manufacturers. In efforts to pursue efficient ANC systems, various improvement measures have been proposed for the conventional narrowband and broadband ANC systems. The typical approaches for the narrowband ANC system include the delay compensation method [27, 28], bandpass filter method [29], local secondary path estimation method [30–33], filtered-error structure method [34–36], and complex signal representation method [37]. As for the broadband ANC system, the most commonly used improvement approaches are the delayless frequency-domain adaptive filtering method [38–40] and the delayless subband adaptive filtering method [8, 38, 41–43].

In addition, a multi-channel ANC system equipped with multiple secondary sources and error microphones needs to be utilized in order to achieve large three-dimensional spatial noise suppression. The conventional multi-channel ANC system is based on the centralized control strategy with good global noise attenuation performance [11, 44, 45]. Nevertheless, the computational complexity of the system increases largely when the number of channels increases. To alleviate the computational burden of multi-channel ANC systems, the decentralized control strategy [46–48] and

the distributed control strategy [41, 49–52] have been widely investigated. This study focuses on analyzing and discussing the methods to reduce the computational complexity of the system in [27–43]; and therefore, it is based on single-channel systems.

As described above, ANC technique has been developed extensively, and some review papers on ANC have been published [12, 53–56]. However, few of them focus on the problem of computational savings. The motivation for this paper is therefore to survey some typical computationally efficient narrowband ANC systems and broadband ANC systems, respectively. The computational complexity of the considered systems is analyzed and compared. Furthermore, to explore the impact caused by reducing computational complexity, the convergence speed and noise reduction performance of the systems are also investigated. This paper is organized as follows. In Sects. 2 and 3, typical computationally efficient narrowband and broadband ANC systems are reviewed, respectively, and the computational complexity analysis is provided. Section 4 evaluates the convergence speed and noise reduction performance of the systems by numerical simulations. Finally, conclusions are summarized in Sect. 5.

## 2 Computationally efficient narrowband ANC systems

### 2.1 Conventional FX-NANC system

Firstly, the conventional narrowband ANC system namely the FX-NANC system is introduced. In Fig. 1,  $P(z)$  is the true primary path,  $S(z)$  is the true secondary path,  $\hat{S}(z)$  is the estimate of the true secondary path,  $d(n)$  is the primary noise signal,  $e(n)$  is the residual noise signal, and the other symbol definitions are given in the following derivation.

The cosine and sine reference signals corresponding to the frequency  $\omega_i$  of the  $i$ th tonal component are expressed as

$$x_{ai}(n) = \cos(\omega_i n) \quad (1)$$

$$x_{bi}(n) = \sin(\omega_i n) \quad (2)$$

and then when there are  $q$  tonal components to be controlled, the total output of all the adaptive notch filters may be given by

$$y(n) = \sum_{i=1}^q y_i(n) = \sum_{i=1}^q [\hat{a}_i(n)x_{ai}(n) + \hat{b}_i(n)x_{bi}(n)] \quad (3)$$

where  $\{\hat{a}_i(n), \hat{b}_i(n)\}_{i=1}^q$  are the weights of the control filters, and  $n$  is the time (or sample point) index.

The residual error signal of the system is defined as

$$e(n) = d(n) - \sum_{m=0}^{M-1} s_m y(n-m) \quad (4)$$

where  $\{s_m\}_{m=0}^{M-1}$  are the impulse response coefficients of the true secondary path  $S(z)$  with length  $M$ .

Based on the FXLMS algorithm, the instantaneous squared error signal is minimized and the weights of the control filters are updated as

$$\hat{a}_i(n + 1) = \hat{a}_i(n) - \frac{\mu_i}{2} \frac{\partial e^2(n)}{\partial \hat{a}_i(n)} \tag{5}$$

$$\hat{b}_i(n + 1) = \hat{b}_i(n) - \frac{\mu_i}{2} \frac{\partial e^2(n)}{\partial \hat{b}_i(n)} \tag{6}$$

for  $i = 1, 2, \dots, q$ , where  $\{\mu_i\}_{i=1}^q$  are the step sizes, and

$$\frac{\partial e^2(n)}{\partial \hat{a}_i(n)} = -2e(n) \sum_{m=0}^{M-1} s_m \frac{\partial y(n-m)}{\partial \hat{a}_i(n)} \approx -2e(n) \sum_{m=0}^{\hat{M}-1} \hat{s}_m x_{ai}(n-m) \tag{7}$$

$$\frac{\partial e^2(n)}{\partial \hat{b}_i(n)} = -2e(n) \sum_{m=0}^{M-1} s_m \frac{\partial y(n-m)}{\partial \hat{b}_i(n)} \approx -2e(n) \sum_{m=0}^{\hat{M}-1} \hat{s}_m x_{bi}(n-m) \tag{8}$$

where  $\{\hat{s}_m\}_{m=0}^{\hat{M}-1}$  are the impulse response coefficients of the estimated secondary path  $\hat{S}(z)$  with length  $\hat{M}$  and may be used to replace  $\{s_m\}_{m=0}^{M-1}$ . And it should be noted that the derivation of Eqs. (7) and (8) contains an assumption that  $\hat{a}_i(n) \approx \hat{a}_i(n-m)$  and  $\hat{b}_i(n) \approx \hat{b}_i(n-m)$  for slow convergence.

Finally, the formulas of updating the control filter weights are rewritten as

$$\hat{a}_i(n + 1) = \hat{a}_i(n) + \mu_i e(n) x'_{ai}(n) \tag{9}$$

$$\hat{b}_i(n + 1) = \hat{b}_i(n) + \mu_i e(n) x'_{bi}(n) \tag{10}$$

where  $x'_{ai}(n)$  and  $x'_{bi}(n)$  are the filtered reference signals and expressed as

$$x'_{ai}(n) = \sum_{m=0}^{\hat{M}-1} \hat{s}_m x_{ai}(n-m) \tag{11}$$

$$x'_{bi}(n) = \sum_{m=0}^{\hat{M}-1} \hat{s}_m x_{bi}(n-m) \tag{12}$$

From Eqs. (9) and (12), it can be observed that the weight updating based on the FXLMS algorithm originally requires only 3 multiplications per input sample in each frequency channel, while the generation of the filtered reference signals requires  $2\hat{M}$  multiplications. The length of the estimated secondary path usually needs to be large enough such as  $\hat{M} = 256$  to ensure that the estimated model can accurately characterize the true secondary path. Therefore, the length  $\hat{M}$  imposes a huge computational burden on the FX-NANC system. On the other hand, when the target noise is a multi-harmonic noise generated by rotating machinery, the number  $q$  of the controlled tonal components is also large. As a result,  $2q\hat{M}$  multiplications per input sample are required for the reference-filtering operations, and the length  $\hat{M}$  and the number  $q$  are considered as the main sources of computational complexity for the FX-NANC system. To improve the computational efficiency of this system especially for

non-stationary noise scenarios, some efforts may be made in relieving the computational requirements for reference filtering.

### 2.2 DFX-NANC system

The delay compensation method proposed by Ziegler [27] is the earliest method used to reduce the computational cost of reference-filtering operations. It employs the delay estimation of the secondary path to substitute the secondary path and use a certain number of delay samples to represent the delay estimation. In other words, this method simplifies the convolution operations of reference filtering to pure sample delay operations, which significantly reduces the computational effort of the narrowband ANC system. The corresponding improved system is called delay FX-NANC (DFX-NANC) system, as illustrated in Fig. 3.

Assuming that the corresponding phase-frequency response of the estimated secondary path at the controlled frequency  $\omega_i$  is represented by  $\hat{\varphi}_{si}$  (since the secondary path only plays the role of delay rather than advance prediction in phase,  $\hat{\varphi}_{si}$  should be kept in the range of  $[-2\pi, 0]$ ), the number of delay samples at  $\omega_i$  may be calculated by

$$\beta_{si} = \text{round}\left(\frac{-\hat{\varphi}_{si}}{\omega_i}\right) \tag{13}$$

Accordingly, the filtered reference signals in the DFX-NANC system are expressed by

$$x'_{ai}(n) = x_{ai}(n - \beta_{si}) \tag{14}$$

$$x'_{bi}(n) = x_{bi}(n - \beta_{si}) \tag{15}$$

From Eqs. (14) and (15), it can be easily seen that the reference-filtering operations do not need to perform any multiplications or additions, and thus the DFX-NANC system has notably less computational cost with respect to the FX-NANC system. However, when the controlled frequency  $\omega_i$  is high, the number of delay samples  $\beta_{si}$  cannot accurately characterize the delay estimation of the secondary path, which may lead to the deterioration of the convergence speed and noise attenuation performance of the

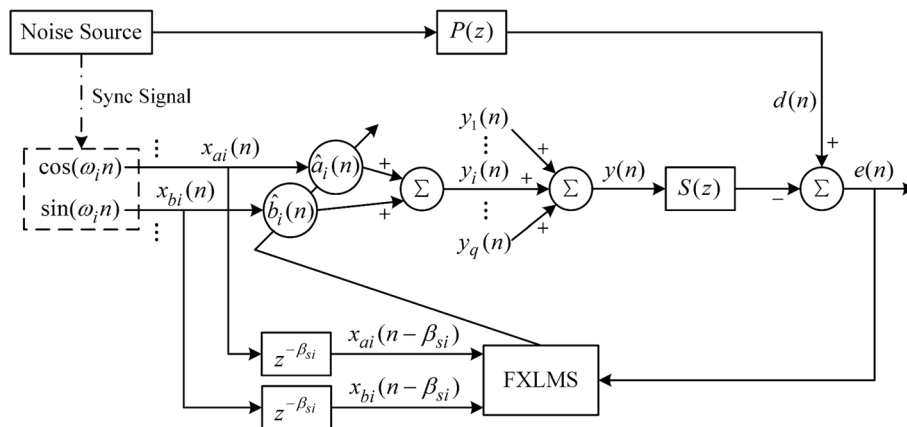


**Fig. 3** Block diagram of the DFX-NANC system (ith channel)

system. Besides, the amplitude effect of the secondary path is not considered at all in the delay compensation method.

### 2.3 BFX-NANC system

In [29], Xiao proposed a bandpass filter bank-based FX-NANC (BFX-NANC) system. With the use of bandpass filter bank, only two convolution operations for reference filtering need to be performed for all the frequency channels. It is realized by the following strategy: Firstly, all the cosine reference signals and all the sine reference signals are summed respectively; and then, the resulting summed reference signals are filtered by the estimation secondary path to generate the total filtered reference signals; finally, the total filtered reference signals are decomposed by the bandpass filters and a series of individual filtered reference signals are obtained.

The block diagram of the BFX-NANC system is shown in Fig. 4. The sum of the cosine reference signals and the sum of the sine reference signals for all the controlled frequencies are expressed respectively by

$$x_a = \sum_{i=1}^q x_{ai} \tag{16}$$

$$x_b = \sum_{i=1}^q x_{bi} \tag{17}$$

and then these two summed reference signals are filtered by the estimated secondary path, as

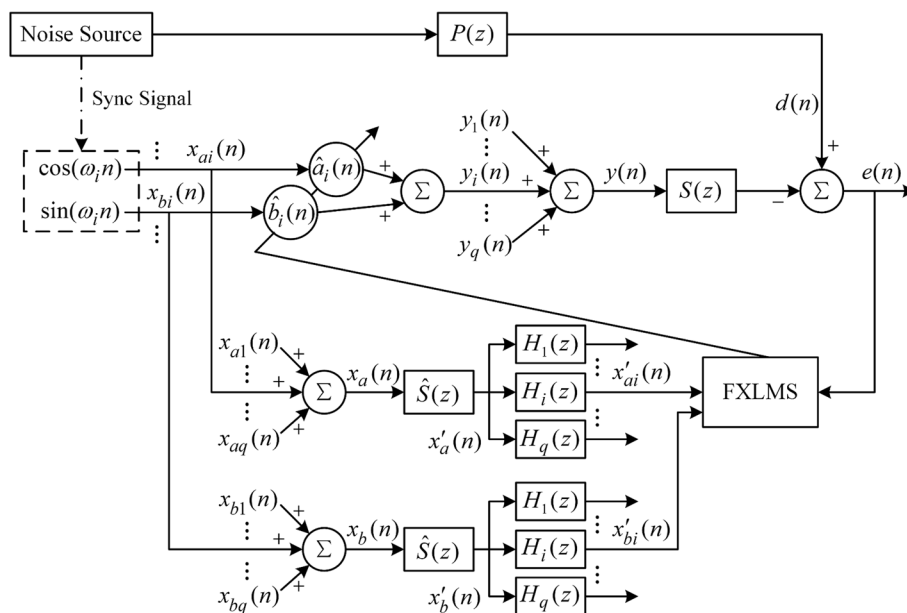


Fig. 4 Block diagram of the BFX-NANC system (ith channel)

$$x'_a(n) = \sum_{m=0}^{\hat{M}-1} \hat{s}_m x_a(n-m) \tag{18}$$

$$x'_b(n) = \sum_{m=0}^{\hat{M}-1} \hat{s}_m x_b(n-m) \tag{19}$$

By using a bank of bandpass filters derived from a second-order IIR notch filter [57], the individual filtered reference signals corresponding to the frequency  $\omega_i$  are calculated by

$$x'_{ai}(n) = (\rho - 1)c_i x_{ai}(n-1) + (\rho^2 - 1)x_{ai}(n-2) - \rho c_i x_{ai}(n-1) - \rho^2 x_{ai}(n-2) \tag{20}$$

$$x'_{bi}(n) = (\rho - 1)c_i x_{bi}(n-1) + (\rho^2 - 1)x_{bi}(n-2) - \rho c_i x_{bi}(n-1) - \rho^2 x_{bi}(n-2) \tag{21}$$

where the transfer function of the bandpass filter used is given by

$$H_i(z) = \frac{(\rho - 1)c_i z^{-1} + (\rho^2 - 1)z^{-2}}{1 + \rho c_i z^{-1} + \rho^2 z^{-2}} \tag{22}$$

$c_i = -2\cos\omega_i$  is the frequency-dependent coefficient and  $0 < \rho < 1$  is the pole-attraction parameter.

On the basis of the above strategy, only two convolution operations are required for reference filtering in the whole BFX-NANC system, and thus the system has less computational cost compared to the FX-NANC system. Nevertheless, as shown in Eqs. (20) and (21), the system needs eight additional multiplications due to the bandpass filters, and at the same time the bandpass filters may also cause some convergence delay.

### 2.4 LFX-NANC system

Generally, the global secondary path over the entire frequency range (the maximum frequency is actually the Nyquist frequency) is modeled using a long FIR filter based on the random white noise method. To reduce the length of the modeling filter, Delgà et al. [30] employed the bandpass filters with the same structure as in Sect. 2.3 and proposed a local secondary path estimation method. The idea behind this method is that the global secondary path can be divided into multiple local secondary paths according to frequency subbands, and correspondingly the single high-order global model can be replaced by a set of low-order local models. It is assumed that the entire frequency range is divided into  $K$  subbands and the local secondary path estimates are represented by  $\hat{S}_k(z)$ ,  $k = 1, 2, \dots, K$ . Then, if the frequency  $\omega_i$  lies in the  $k$ th subband, the corresponding local model is denoted by  $\hat{S}_{ki}(z)$ . The block diagram of the local secondary path estimation based FX-NANC (LFX-NANC) system is presented in Fig. 5. The expressions of the filtered reference signals in the system are written as



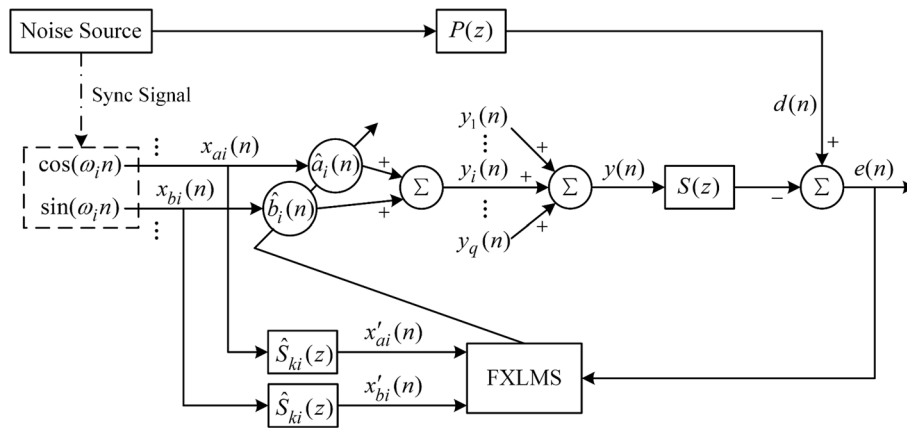


**Fig. 5** Block diagram of the LFX-NANC system (*l*th channel)

$$x'_{ai}(n) = \sum_{m=0}^{\hat{M}_l-1} \hat{s}_{k,m} x_{ai}(n-m) \tag{23}$$

$$x'_{bi}(n) = \sum_{m=0}^{\hat{M}_l-1} \hat{s}_{k,m} x_{bi}(n-m) \tag{24}$$

where  $\{\hat{s}_{k,m}(n)\}_{m=0}^{\hat{M}_l-1}$  are the impulse response coefficients of the local secondary path model  $\hat{S}_k(z)$  (or  $\hat{S}_{ki}(z)$ ) with length  $\hat{M}_l$ .

The length  $\hat{M}_l$  can be taken as a much smaller value compared to the length  $\hat{M}$  of  $\hat{S}(z)$  ( $\hat{M}_l \leq \hat{M}$ ), and thus the computational load of reference filtering in the LFX-NANC system is greatly decreased. But it was shown in [32, 33] that Delegà's local secondary path estimation method cannot guarantee good spectral estimation accuracy at most frequencies of each subband, especially when the dynamic range of amplitude-frequency response of the secondary path is large. Therefore, the convergence performance of the LFX-NANC system may be limited.

### 2.5 FE-NANC system

Considering different algorithm structures, Zhu et al. [34] adopted the filtered-error structure instead of the usual filtered-reference structure to develop a filtered-error least mean square (FELMS) based narrowband ANC (FE-NANC) system. The block diagram of the FE-NANC system is shown in Fig. 6, where  $\hat{S}'(z)$  is the error filter. In this system, the sole error signal is filtered by the error filter, and then the filtered error signal is used to update the control filter weights in all the frequency channels. Accordingly, only one convolution operation for error filtering is required in the whole FE-NANC system, regardless of the number of tonal components. Defining two expressions as follows:

$$\Delta g_a(n) = e(n) \sum_{m=0}^{\hat{M}-1} \hat{s}_m x_{ai}(n-m) \tag{25}$$

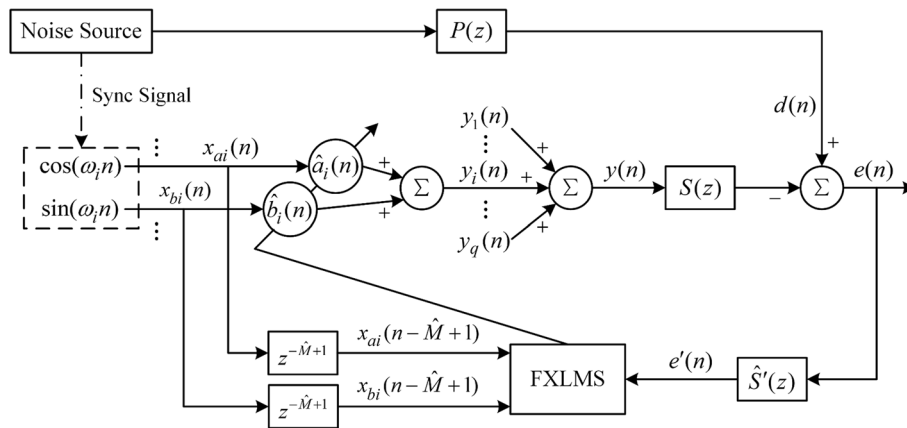


**Fig. 6** Block diagram of the FE-NANC system (*i*th channel)

$$\Delta g_b(n) = e(n) \sum_{m=0}^{\hat{M}-1} \hat{s}_m x_{bi}(n - m) \tag{26}$$

Let  $v = n - m$ , thereby Eqs. (25) and (26) are rewritten as

$$\Delta g_a(v) = \sum_{m=0}^{\hat{M}-1} \hat{s}_m e(v + m) x_{ai}(v) \tag{27}$$

$$\Delta g_b(v) = \sum_{m=0}^{\hat{M}-1} \hat{s}_m e(v + m) x_{bi}(v) \tag{28}$$

Since  $\sum_{m=0}^{\hat{M}-1} \hat{s}_m e(v + m)$  cannot be implemented with a causal system,  $e(v + m)$ ,  $x_{ai}(v)$  and  $x_{bi}(v)$  are delayed by  $\hat{M} - 1$  samples. Then

$$\Delta g_a(v) = \sum_{m=0}^{\hat{M}-1} \hat{s}_m e(v + m - \hat{M} + 1) x_{ai}(v - \hat{M} + 1) \tag{29}$$

$$\Delta g_b(v) = \sum_{m=0}^{\hat{M}-1} \hat{s}_m e(v + m - \hat{M} + 1) x_{bi}(v - \hat{M} + 1) \tag{30}$$

Defining  $j = \hat{M} - 1 - m$  and

$$e'(v) = \sum_{j=0}^{\hat{M}-1} \hat{s}_{\hat{M}-1-j} e(v - j) \tag{31}$$

where  $\{\hat{s}_{\hat{M}-1}, \hat{s}_{\hat{M}-2}, \dots, \hat{s}_0\}$  may be considered as the weights of the error filter  $\hat{S}'(z)$ .

Finally, the control filter weights of the FE-NANC system are updated by

$$\hat{a}_i(n + 1) = \hat{a}_i(n) + \mu_i e'(n) x_{ai}(n - \hat{M} + 1) \tag{32}$$

$$\hat{b}_i(n + 1) = \hat{b}_i(n) + \mu_i e'(n) x_{bi}(n - \hat{M} + 1) \tag{33}$$

where  $e'(n)$  denotes the filtered error signal, and the formulas are based on the assumptions:  $e'(n) \approx e'(v)$ ,  $x_{ai}(n - \hat{M} + 1) \approx x_{ai}(v - \hat{M} + 1)$  and  $x_{bi}(n - \hat{M} + 1) \approx x_{bi}(v - \hat{M} + 1)$ . It is noted that the length  $\hat{M}$  of the estimated secondary path plays an important role in the above sample delay operation and assumptions. This indicates that the convergence speed of the FE-NANC system may be very poor when  $\hat{M}$  takes a large value.

### 2.6 LFE-NANC system

Based on the local secondary path estimation method, an improved FE-NANC (called LFE-NANC) system is developed in our recent study [32, 33], as shown in Fig. 7. The LFE-NANC system differs from the above FE-NANC system in that a set of local secondary path estimates are used. Furthermore, the local models are obtained by the improved local secondary path modeling methods that are more accurate than Delgà's modeling method. On the basis of this, the LFE-NANC system may have not only less computational cost but also much better convergence performance than the FE-NANC system.

Correspondingly, the control filter weights of the LFE-NANC system are updated using the FELMS algorithm, as

$$\hat{a}_i(n + 1) = \hat{a}_i(n) + \mu_i e'_i(n) x_{ai}(n - \hat{M}_l + 1) \tag{34}$$

$$\hat{b}_i(n + 1) = \hat{b}_i(n) + \mu_i e'_i(n) x_{bi}(n - \hat{M}_l + 1) \tag{35}$$

where

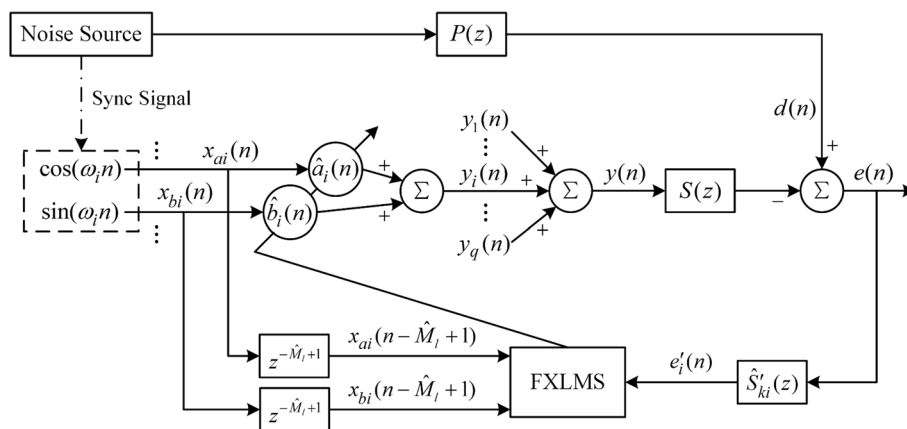


**Fig. 7** Block diagram of the LFE-NANC system (*i*th channel)

$$e'_i(n) = \sum_{j=0}^{\hat{M}_i-1} \hat{s}_{\hat{M}_i-1-j} e(n-j) \tag{36}$$

**2.7 CFX-NANC system**

The above narrowband ANC systems are all based on real-valued signals, which is consistent with real-world applications. Considering that two complex-conjugate sinusoidal signals can be merged into a real-valued sinusoidal signal, Jeon et al. [37] proposed a complex FXLMS algorithm-based narrowband ANC (CFX-NANC) system. The CFX-NANC system uses the complex signal representation method to convert the convolution operation for reference filtering at a controlled frequency into the complex-valued multiplication operation. There is no doubt that the computational complexity of the system can be significantly improved. The reference signals in this system are expressed by

$$x_{ai}(n) = e^{j(\omega_i n - \pi/2)} \tag{37}$$

$$x_{bi}(n) = e^{-j(\omega_i n - \pi/2)} \tag{38}$$

Then the filtered reference signals are given by

$$x'_{ai}(n) = \hat{A}_{si} e^{j\hat{\varphi}_{si}} x_{ai}(n) \tag{39}$$

$$x'_{bi}(n) = \hat{A}_{si} e^{j\hat{\varphi}_{si}} x_{bi}(n) \tag{40}$$

where  $\hat{A}_{si}$  and  $\hat{\varphi}_{si}$  are the amplitude gain and phase shift of the estimated secondary path  $\hat{S}(z)$  at the frequency  $\omega_i$ , respectively.

The control filter weights are updated by the complex FXLMS algorithm, as

$$\hat{a}_i(n+1) = \hat{a}_i(n) + \mu_i e^*(n) x'_{ai}(n) \tag{41}$$

$$\hat{b}_i(n+1) = \hat{b}_i(n) + \mu_i e^*(n) x'_{bi}(n) \tag{42}$$

where  $(\blacksquare)^*$  denotes the complex conjugate operation. It can be seen that the CFX-NANC system involves a series of complex-valued operations, although the complex time-domain convolutions are replaced by the simple frequency-domain multiplications.

**2.8 Computational complexity analysis**

In this section, the computational complexity of the conventional FX-NANC system, DFX-NANC system, BFX-NANC system, LFX-NANC system, FE-NANC system, LFE-NANC system, and CFX-NANC system is analyzed and compared. Table 1 summarizes the required number of real multiplications per input sample for the seven systems. It is assumed that one complex multiplication is equivalent to four real multiplications. As defined earlier,  $q$  represents the number of controlled frequencies,  $\hat{M}$  and  $\hat{M}_l$  represent the length of global and local secondary path estimates, respectively.

**Table 1** Computational complexity of the seven narrowband ANC systems in terms of real multiplications

	FX-NANC	DFX-NANC	BFX-NANC	LFX-NANC	FE-NANC	LFE-NANC	CFX-NANC
Controller output	$2q$	$2q$	$2q$	$2q$	$2q$	$2q$	$8q$
Reference filtering	$2q\hat{M}$	0	$2\hat{M} + 8q$	$2q\hat{M}_l$	$\hat{M}$	$q\hat{M}_l$	$8q$
Weight updating	$3q$	$3q$	$3q$	$3q$	$3q$	$3q$	$10q$
Total	$2q\hat{M} + 5q$	$5q$	$2\hat{M} + 13q$	$2q\hat{M}_l + 5q$	$\hat{M} + 5q$	$q\hat{M}_l + 5q$	$26q$

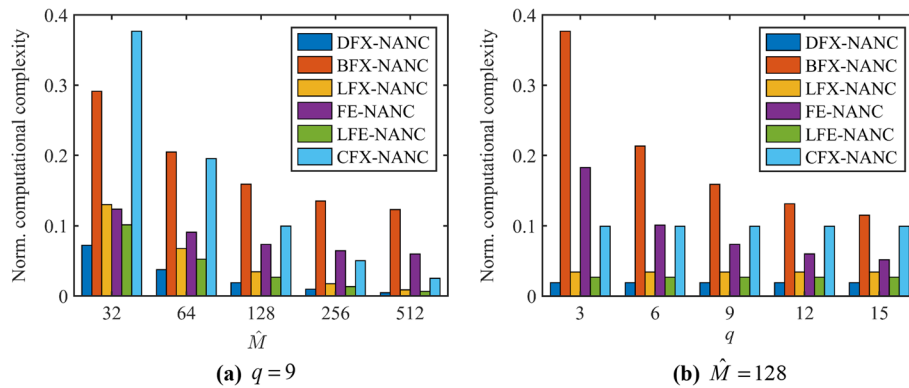


**Fig. 8** Normalized computational complexity of the six computationally efficient narrowband ANC systems for different  $\hat{M}$  and  $q$  with respect to the conventional FX-NANC system

The normalized computational complexity of the six computationally efficient narrowband ANC systems for different  $\hat{M}$  and  $q$  with respect to the conventional FX-NANC system is compared quantitatively in Fig. 8, where  $\hat{M}_l$  is set to 2. It is obvious from Fig. 8 that in all the considered typical cases, the computational complexity of the DFX-NANC system and the LFE-NANC system is always less than 10% of the conventional system. The DFX-NANC system enjoys the best computational advantage among all the systems, and the LFE-NANC system is the second system with the lowest computational complexity. And when  $\hat{M}$  and  $q$  take smaller values, the computational merit of the BFX-NANC system and the CFX-NANC system is not very significant compared to other systems. In a usual case of  $\hat{M} = 128$  and  $q = 9$ , the six computationally efficient narrowband ANC systems can save the number of performed real multiplications by 98.1%, 84.1%, 96.6%, 92.6%, 97.3%, 90.0%, respectively, and thus the comparative results of the computational merit of these systems may be expressed as DFX-NANC > LFE-NANC > LFX-NANC > FE-NANC > CFX-NANC > BFX-NANC.

### 3 Computationally efficient broadband ANC systems

#### 3.1 Conventional FX-BANC system

Before introducing computationally efficient broadband ANC systems, the conventional FX-BANC system in Fig. 2 is first reviewed as follows:

The output of the control filter  $W(z)$  is given by

$$y(n) = \mathbf{w}^T(n)\mathbf{x}(n) \tag{43}$$

where  $\mathbf{w}(n)$  and  $\mathbf{x}(n)$  are the control filter weight vector and reference signal vector respectively, defined as

$$\mathbf{w}(n) = [w_0(n), w_1(n), \dots, w_{N-1}(n)]^T \quad (44)$$

$$\mathbf{x}(n) = [x(n), x(n-1), \dots, x(n-N+1)]^T \quad (45)$$

$N$  is the length of the control filter.

The formula of updating the weight vector for the FX-BANC system may be expressed by

$$\mathbf{w}(n+1) = \mathbf{w}(n) + \mu e(n) \mathbf{x}'(n) \quad (46)$$

where  $\mu$  is the step size,  $\mathbf{x}'(n)$  is the filtered reference signal vector and written as

$$\mathbf{x}'(n) = [x'(n), x'(n-1), \dots, x'(n-N+1)]^T \quad (47)$$

$$x'(n) = \sum_{m=0}^{\hat{M}-1} \hat{s}_m x(n-m) \quad (48)$$

This FX-BANC system is actually the most basic system for active noise control. On the basis of this system, the normalized FXLMS algorithm-based broadband ANC (NFX-BANC) system is developed by normalizing the step size according to the power of the filtered reference signal. The NFX-BANC system employs the normalized step size and thus its convergence performance may be improved in the case of the reference signal with large power spectra disparity. Accordingly, the weight vector of the NFX-BANC system is updated by the normalized FXLMS algorithm, as

$$\mathbf{w}(n+1) = \mathbf{w}(n) + \frac{\mu}{\mathbf{x}'^T(n) \mathbf{x}'(n) + \varepsilon} e(n) \mathbf{x}'(n) \quad (49)$$

where  $\varepsilon$  is a small regularization constant to avoid the denominator being too small.

Since a transversal FIR filter is used as the control filter, the FX-BANC system involves two convolution operations per input sample, including the control filtering and filtered reference vector generation. As can be seen from Eqs. (43) and (48) that the number of performed multiplications regarding convolution operations of the system depends on the length  $N$  of the control filter and the length  $\hat{M}$  of the estimated secondary path. As for the NFX-BANC system, the normalization of the step size will increase another  $N$  multiplications. To reduce the computational cost, several frequency-domain methods and subband methods have been proposed.

### 3.2 DF-BANC system

Based on the frequency-domain implementation of the LMS algorithm in [58], Zhang et al. [59] proposed a normalized frequency-domain block filtering method, and the corresponding broadband ANC system is called FB-BANC system as given in Fig. 9. Instead of the conventional point-based processing, the frequency-domain block filtering method can process the signal block by block and perform a time-domain convolution

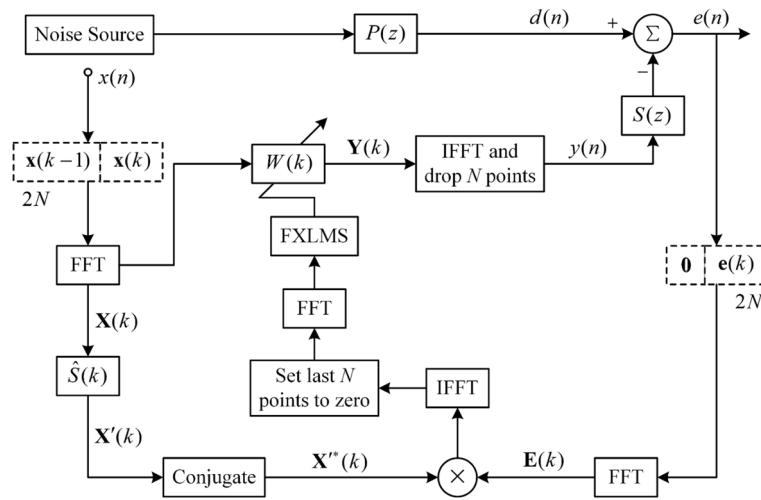


**Fig. 9** Block diagram of the FB-BANC system

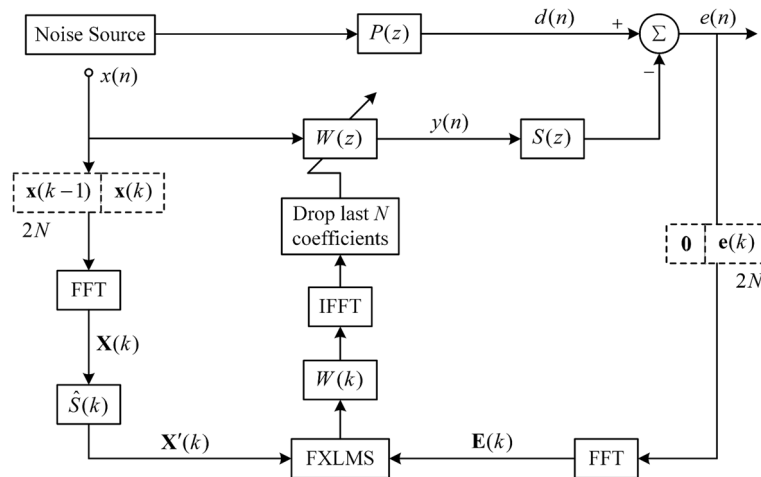


**Fig. 10** Block diagram of the DF-BANC system

via a frequency-domain multiplication based on the fast Fourier transform (FFT) and the overlap-save method. In this way, the high computational complexity resulting from large lengths of the control filter and the estimated secondary path may be reduced. However, in the FB-BANC system, the control filtering is also implemented in frequency domain, which inevitably causes a delay of one block length. The effect of the undesired delay is extremely unfavorable for broadband noise control. To this end, a delay-less frequency-domain filtering based broadband ANC (DF-BANC) system is developed according to the studies [38–40]. Figure 10 shows the block diagram of the DF-BANC system. In this system, the control filtering is implemented directly in time domain to minimize the delay; while, the weight vector is updated in frequency domain and then the modified frequency-domain weight vector is transformed to update the time-domain weight vector by the inverse FFT (IFFT).

The control filter output in the DF-BANC system is expressed by

$$y(n) = \mathbf{w}^T(k)\mathbf{x}(n) \tag{50}$$

where  $(\mathbf{a})^T$  denotes the transpose operation,  $k$  is the block index,  $\mathbf{w}(k)$  and  $\mathbf{x}(n)$  are the control filter weight vector and reference signal vector in time domain respectively, defined as

$$\mathbf{w}(k) = [w_0(k), w_1(k), \dots, w_{N-1}(k)]^T \tag{51}$$

$$\mathbf{x}(n) = [x(n), x(n - 1), \dots, x(n - N + 1)]^T \tag{52}$$

Assuming that the length of each data block is equal to the length  $N$  of the control filter  $W(z)$ , then the  $k$ th data block for  $x(n)$ ,  $y(n)$  and  $e(n)$  are written as

$$\mathbf{x}(k) = [x(kN - N + 1), x(kN - N + 2), \dots, x(kN)]^T \tag{53}$$

$$\mathbf{y}(k) = [y(kN - N + 1), y(kN - N + 2), \dots, y(kN)]^T \tag{54}$$

$$\mathbf{e}(k) = [e(kN - N + 1), e(kN - N + 2), \dots, e(kN)]^T \tag{55}$$

The overlap-save method (50% overlap) is used to convert the circular correlation due to FFT processing to desired linear correlation, and thus two blocks of all the time-domain signals to be processed need to be concatenated to form a  $2N$ -point data vector for frequency-domain calculations. It is worth noting that the  $(k - 1)$ th block of the error signal needs to be padded with a zero vector of length  $N$  to form a  $2N$ -point data vector. On the basis of this, the weight vector of the control filter is updated in frequency domain using the complex normalized FXLMS algorithm, as

$$W_m(k + 1) = W_m(k) + \frac{\mu}{X_m'^*(k)X_m'(k) + \varepsilon} E_m(k)X_m'^*(k) \tag{56}$$

where  $(\mathbf{a})^*$  denotes the complex conjugate operation,  $m = 0, 1, \dots, N - 1$ , is the frequency-bin index,  $W_m(k)$ ,  $E_m(k)$ , and  $X_m'(k)$  are the control filter weight, the error signal and the filtered reference signal in the  $m$ th frequency-bin, and the corresponding frequency-domain vectors may be expressed by

$$\mathbf{W}(k) = [W_0(k), W_1(k), \dots, W_{2N-1}(k)]^T \tag{57}$$

$$\mathbf{E}(k) = \text{FFT} \left\{ \left[ \mathbf{0}^T, \mathbf{e}^T(k) \right]^T \right\} = [E_0(k), E_1(k), \dots, E_{2N-1}(k)]^T \tag{58}$$

$$\mathbf{X}'(k) = \hat{\mathbf{S}}(k)\mathbf{X}(k) \tag{59}$$

$$\mathbf{S}(k) = \text{FFT} \left\{ [\hat{s}_0, \hat{s}_1, \dots, \hat{s}_{\hat{M}-1}]^T \right\}_{2N} = [S_0(k), S_1(k), \dots, S_{2N-1}(k)]^T \tag{60}$$



$$\mathbf{X}(k) = \text{FFT} \left\{ \left[ \mathbf{x}^T(k-1), \mathbf{x}^T(k) \right]^T \right\} = [X_0(k), X_1(k), \dots, X_{2N-1}(k)]^T \quad (61)$$

Finally, the time-domain weight vector  $\mathbf{w}(k)$  is updated based on the frequency-domain weight vector  $\mathbf{W}(k)$ , as

$$\mathbf{w}(k+1) = \text{first } N \text{ coefficients of } \text{IFFT} \{ \mathbf{W}(k+1) \} = [w_0(k+1), w_1(k+1), \dots, w_{N-1}(k+1)]^T \quad (62)$$

and  $\mathbf{W}(k)$  and  $\mathbf{w}(k)$  are both updated only once for every  $N$  input samples.

### 3.3 DS-BANC system

In addition to the delayless frequency-domain filtering method, the delayless subband filtering method is currently a more popular method for reducing the computational complexity of broadband ANC systems [8, 38, 41, 42]. Figure 11 illustrates the block diagram of a delayless subband filtering based broadband ANC (DS-BANC) system. In the DS-BANC system, the filtered reference signal and the error signal are both decomposed into  $G$  subbands by an analysis filter bank  $\mathbf{H}(z)$  and decimated by factor  $D$ . The analysis filter bank consists of  $G$  bandpass filters and is usually based on the polyphase FFT technique instead of complex time-domain convolutions to calculate the subband signals. The resulting subband filtered reference signals and error signals are used to update the corresponding subband control filter weights. For the  $i$ th subband control filter, the weight vector may be updated using the complex normalized FXLMS algorithm, as

$$\mathbf{w}_i(n+D) = \mathbf{w}_i(n) + \frac{\mu}{[\mathbf{x}'_i(n)]^H \mathbf{x}'_i(n) + \varepsilon} e_i(n) \mathbf{x}'_i(n)^* \quad (63)$$

where  $(\mathbf{a})^H$  denotes the Hermitian transpose operation,  $e_i(n)$  is the  $i$ th subband error signal,  $\mathbf{x}'_i(n)$  is the  $i$ th subband filtered reference signal vector,  $\mathbf{w}_i(n)$  is the weight vector of

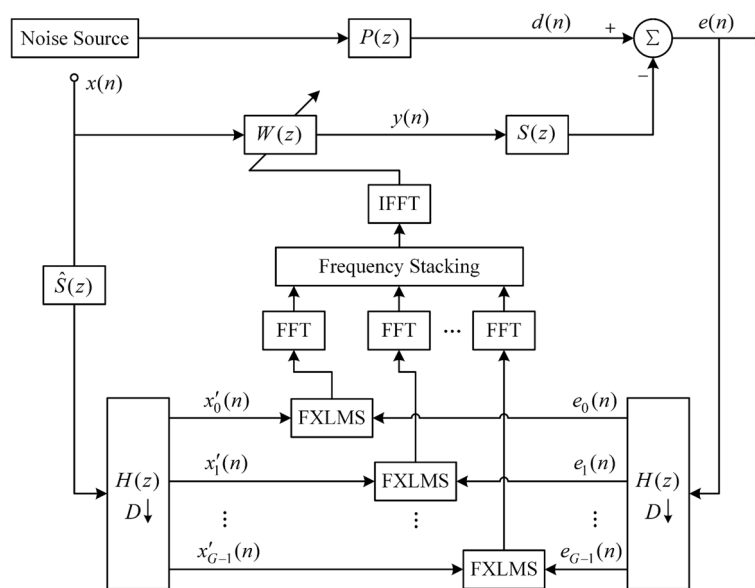


Fig. 11 Block diagram of the DS-BANC system

the  $i$ th subband control filter with length  $N_s = N/D$ , and  $N$  is the length of the fullband control filter.

Since the reference and error signals are real-valued signals, the subbands are complex conjugate symmetric. This means that only the first  $G/2 + 1$  subbands need to be considered for weight updating. After all the updated subband weight vectors are obtained, the fullband weight vector can be constructed by the FFT stacking. Generally, the fullband weight vector is updated only once for every  $N/J$  input samples, and  $J$  is the fullband weight transform rate. It is obvious that the computational cost of the DS-BANC system is largely reduced due to the down-sampling process.

### 3.4 MDS-BANC system

To further reduce the computational complexity, a modified delayless subband filtering method with the use of subband secondary path models is developed [43]. The block diagram of the corresponding broadband ANC system (called MDS-BANC system) is shown in Fig. 12. In the MDS-BANC system, the computational merit is enhanced with respect to that of the DS-BANC system by decomposing the fullband secondary path estimate into a set of subband secondary path estimates with the decimation factor  $D$ .

The subband filtered reference signals are obtained by filtering the reference signal  $x(n)$  through  $\mathbf{H}(z)$  followed by  $\hat{S}_i(z)$ ,  $i=0, 1, \dots, G-1$ .  $\hat{S}_i(z)$  is the  $i$ th subband secondary path estimate and can be modeled using a short FIR filter in a subband-decomposed form. It should be noted that the subband secondary path estimation here is similar to the local secondary path estimation in Sects. 2.4 and 2.6, but the difference is that the subband secondary path estimation is implemented at the decimated sampling frequency. Except for the generation of the subband filtered reference signals, the rest of the MDS-BANC system is the same as the DS-BANC system. On the other hand, both the DS-BANC system and the MDS-BANC system may more easily attenuate the noise over a broadband

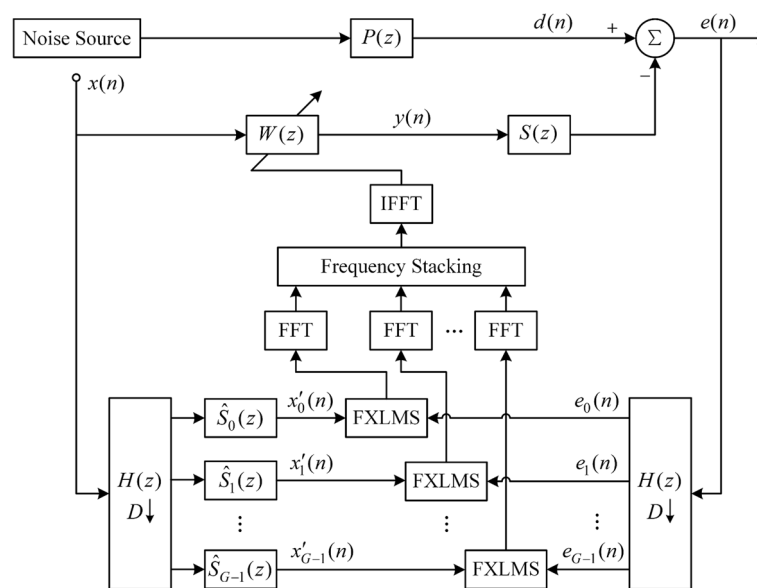


Fig. 12 Block diagram of the MDS-BANC system

frequency range than the conventional FX-BANC system, since each subband control filter can fully play its role in the corresponding narrow frequency band.

### 3.5 Computational complexity analysis

The computational complexity of the NFX-BANC system, DF-BANC system, DS-BANC system and MDS-BANC system is analyzed and compared in this section. Table 2 summarizes the required number of real multiplications per input sample for the four systems. It is assumed that each  $N$ -point FFT or IFFT operation requires  $M\log_2 N$  real multiplications, and one complex multiplication is equivalent to four real multiplications.  $N$  and  $N_s$  represent the length of fullband and subband control filter, respectively,  $\hat{M}$  and  $\hat{M}_s$  represent the length of fullband and subband secondary path estimates, respectively,  $G$  represents the number of subbands,  $D$  represents the decimation factor,  $L$  represents the length of analysis filters, and  $J$  represents the fullband weight transform rate. And some of these parameters typically have the following relationships:  $N_s = N/D$ ,  $\hat{M}_s = \hat{M}/D$ ,  $D = G/2$ .

The normalized computational complexity of the three computationally efficient broadband ANC systems for different  $N$ ,  $\hat{M}$  and  $G$  with respect to the NFX-BANC system is compared quantitatively in Fig. 13, where  $J = 2$  and  $L = 4G$ . The results indicate that the DF-BANC system exhibits the greatest computational superiority among these systems, and the computational complexity of the MDS-BANC system is lower than that of the DS-BANC system. In a usual case of  $N = 256$ ,  $\hat{M} = 256$  and  $G = 32$ , the three computationally efficient broadband ANC systems can save the number of performed real multiplications by 67.0%, 25.2%, and 43.5%, respectively, and thus the comparative results of the computational merit of the systems may be expressed as DF-BANC > MDS-BANC > DS-BANC. Moreover, it can also be seen from Fig. 13c that with the increase in the number of subbands  $G$ , the computational cost of the DS-BANC system and the MDS-BANC system decreases significantly.

## 4 Numerical simulations

To evaluate the convergence speed and noise attenuation performance of all the considered ANC systems with reduced computational complexity, several numerical simulations are carried out in MATLAB environment. Considering that for narrowband noise control, the target noise is usually stationary or non-stationary multi-harmonic noise, two synthesized stationary and non-stationary multi-tonal noises are used as the noise source signals to fully validate the control performance of the narrowband ANC systems [2, 3, 5, 32, 33]. The broadband noise control is generally considered to be more difficult than the narrowband

**Table 2** Computational complexity of the four broadband ANC systems in terms of real multiplications

System	Number of real multiplications
NFX-BANC	$3N + \hat{M} + 1$
DF-BANC	$6 \log_2(2N) + N + 28$
DS-BANC	$\frac{4L}{G} + 4 \log_2 G + \hat{M} + N + \frac{16N}{G} + \frac{32N}{G^2} + \frac{8}{G} + 4 + \left[ \left( \frac{G}{2} + 1 \right) \frac{8}{G} \log_2 \frac{4N}{G} + 2 \log_2(2N) \right] J$
MDS-BANC	$\frac{4L}{G} + 4 \log_2 G + \frac{8\hat{M}}{G} + \frac{16\hat{M}}{G^2} + N + \frac{16N}{G} + \frac{32N}{G^2} + \frac{8}{G} + 4 + \left[ \left( \frac{G}{2} + 1 \right) \frac{8}{G} \log_2 \frac{4N}{G} + 2 \log_2(2N) \right] J$

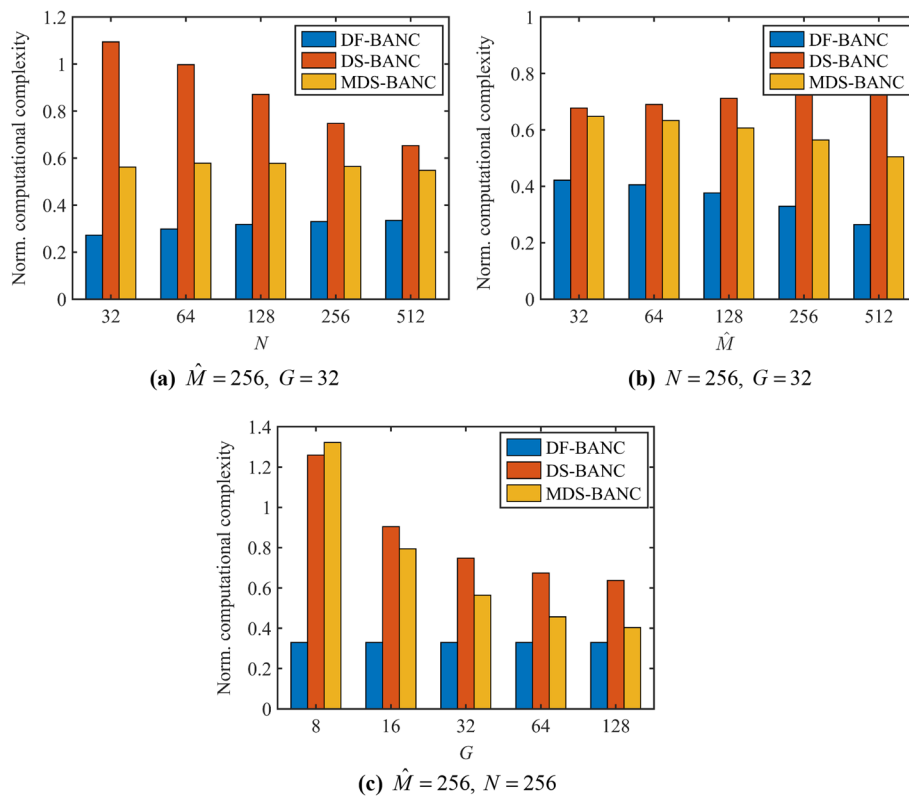


**Fig. 13** Normalized computational complexity of the three computationally efficient broadband ANC systems for different  $N, \hat{M}$  and  $G$  with respect to the NFX-BANC system

noise control, so current ANC research is mainly focused on steady-state broadband noise control [4, 38, 41–43]. To verify the control performance of the broadband ANC systems for broadband noises with different spectral dynamic ranges, both white Gaussian noise and colored noise are used as the noise source signals. The computer used has an Intel Core i5-6300HQ (2.3 GHz) processor and 4 GB RAM. The models of the primary and secondary paths used in the simulations are taken from [9], as illustrated in Fig. 14a, b. The sampling frequency is 2000 Hz. The length  $\hat{M}$  of the global (or fullband) secondary path estimate  $\hat{S}(z)$  is set to 256.

#### 4.1 Performance comparison of narrowband ANC systems

##### 4.1.1 Case 1: Stationary multi-tonal noise

In case 1, a multi-tonal noise with six integer harmonic orders and fundamental frequency of 100 Hz is used as the source noise signal to compare the control performance of the six computationally efficient narrowband ANC systems. The source noise signal is given by

$$\begin{aligned}
 x(n) = & 0.4 \sin\left(2\pi \frac{100}{2000} n\right) + 0.2 \sin\left(2\pi \frac{200}{2000} n\right) + 0.5 \sin\left(2\pi \frac{300}{2000} n\right) + 0.3 \sin\left(2\pi \frac{400}{2000} n\right) \\
 & + 0.6 \sin\left(2\pi \frac{500}{2000} n\right) + 0.4 \sin\left(2\pi \frac{600}{2000} n\right)
 \end{aligned}
 \tag{64}$$

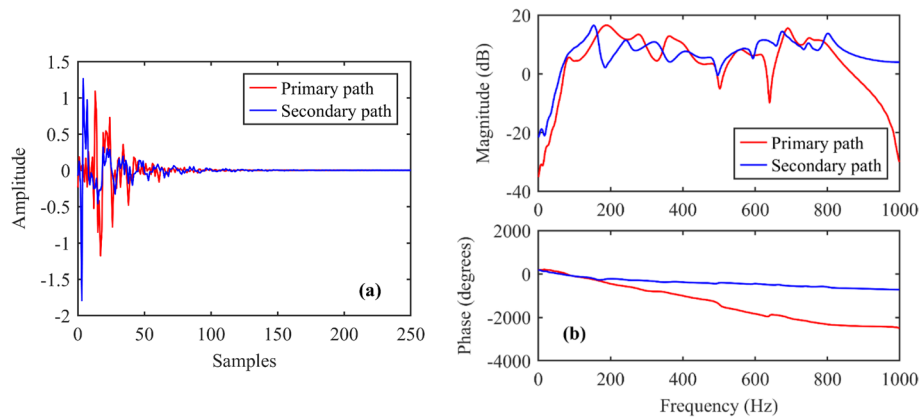


**Fig. 14** Models of the primary and secondary paths used in the simulations. **a** Impulse response functions, **b** frequency response functions

The primary noise signal is generated by this source noise signal and an additional zero-mean white Gaussian noise, expressed as

$$d(n) = \sum_{j=0}^{255} p_j x(n-j) + v_p(n) \tag{65}$$

where  $\{p_j\}_{j=0}^{255}$  are the impulse response coefficients of the primary path  $P(z)$ , the variance of the white noise  $v_p(n)$  is set to 0.02.

The conventional FX-NANC system is used as the benchmark. The length of each simulation is 1 s. The pole-attraction parameter  $\rho$  is set to 0.99. The length of the local secondary path estimates is set to  $\hat{M}_l = 5$ . All the step sizes are carefully adjusted so as to provide fair comparisons between the systems, and multiple independent trials are conducted to obtain ensemble averaged results. Two metrics including the averaged noise reduction (ANR) [43, 60] and the sound pressure level (SPL) are used to evaluate the performance of the systems, and they are defined as follows:

$$\text{ANR}(n) = 20 \log_{10} \left( \frac{A_e(n)}{A_d(n)} \right) \text{ (dB)} \tag{66}$$

where  $A_e(n) = \xi A_e(n-1) + (1-\xi)|e(n)|$ ,  $A_d(n) = \xi A_d(n-1) + (1-\xi)|d(n)|$  with initial conditions  $A_e(0) = 0$ ,  $A_d(0) = 0$ , and  $\xi = 0.999$  is the forgetting factor.

$$\text{SPL} = 20 \log_{10} \left( \frac{P}{P_{\text{ref}}} \right) \text{ (dB)} \tag{67}$$

where  $P$  is the sound pressure to be calculated, and  $P_{\text{ref}} = 2 \times 10^{-5}$  Pa is the reference sound pressure.

Figure 15 presents the comparison of the ANR curves for the seven narrowband ANC systems in this case (the ANR curves of the FX-NANC, BFX-NANC and LFE-NANC systems are overlapped). It is shown that the BFX-NANC and LFE-NANC systems have similar convergence speeds to that of the FX-NANC system, the CFX-NANC system converges faster than the FX-NANC system while the DFX-NANC and LFX-NANC systems converges slower than the FX-NANC system, and the FE-NANC system performs

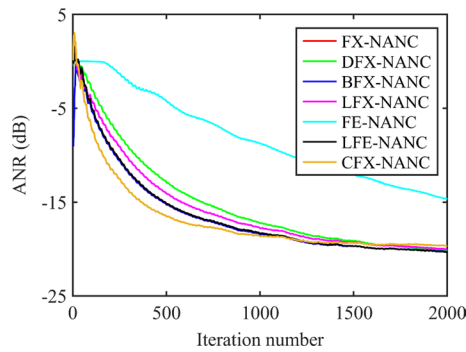


**Fig. 15** Comparison of the ANR curves for the seven narrowband ANC systems in case 1

the worst with severe delay. The results are consistent with those described in Sect. 2. Furthermore, the time waveforms and the frequency spectrums of the residual noise for the seven narrowband ANC systems are depicted in Figs. 16 and 17, respectively. As is presented in Fig. 17, the noise reduction performance of the DFX-NANC system and the FE-NANC system is obviously inferior to other systems.

**4.1.2 Case 2: Non-stationary multi-tonal noise**

This case aims to investigate the ability of the considered narrowband ANC systems to deal with non-stationary primary noise. The source noise signal consists of

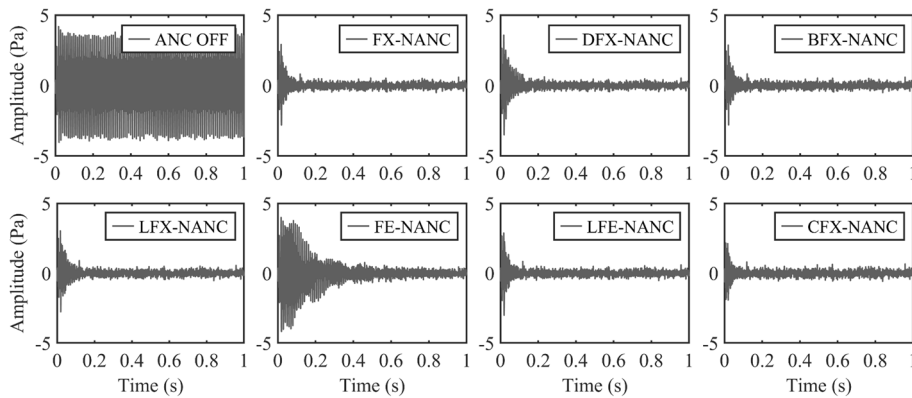


**Fig. 16** Time waveforms of the residual noise for the seven narrowband ANC systems in case 1

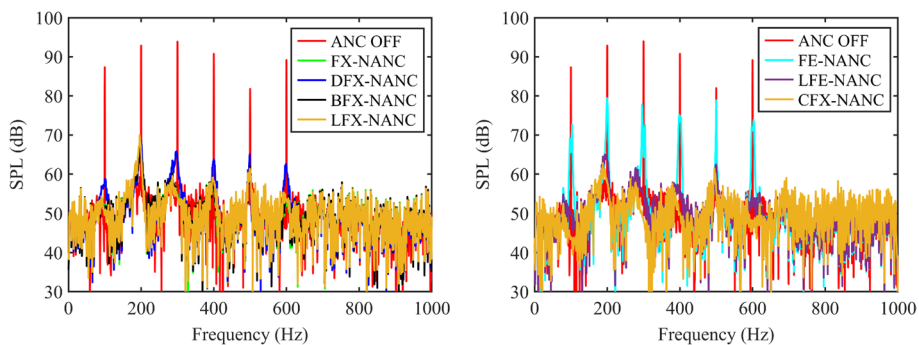


**Fig. 17** Frequency spectrums of the residual noise for the seven narrowband ANC systems in case 1

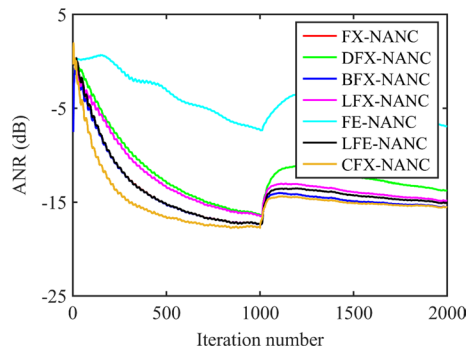


**Fig. 18** Comparison of the ANR curves for the seven narrowband ANC systems in case 2

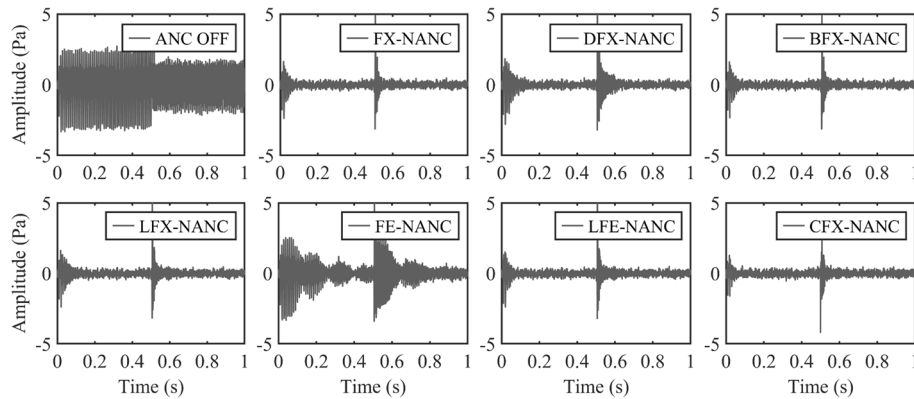


**Fig. 19** Time waveforms of the residual noise for the seven narrowband ANC systems in case 2

three tonal components with frequency of 100 Hz, 200 Hz, and 300 Hz, and their amplitudes are 0.4 Pa, 0.2 Pa and 0.5 Pa, respectively. The duration of the simulation is still 1 s, but the frequency and amplitude of the three tonal components in the source noise signal are changed at the intermediate moment. After the variation, the frequencies of the three tonal components are 400 Hz, 500 Hz, and 600 Hz, and the amplitudes are 0.3 Pa, 0.6 Pa and 0.4 Pa. The rest of the parameter settings are the same as those in case 1.

The comparison of the ANR curves for the seven narrowband ANC systems in case 2 is illustrated in Fig. 18, where the ANR curves of the FX-NANC, BFX-NANC and LFE-NANC systems are overlapped in the first 1000 iterations, and the ANR curves of the FX-NANC and BFX-NANC systems are overlapped in the last 1000 iterations. In addition, the time waveforms of the residual noise for the seven narrowband ANC systems are also given in Fig. 19. The results demonstrate that all of the computationally efficient narrowband ANC systems may track time-varying multi-tonal noise and tackle the variation relatively well, except for the FE-NANC system. Overall, the comparative results of the convergence speed of all the systems may be expressed as  $CFX-NANC > FX-NANC = BFX-NANC = LFE-NANC > LFX-NANC > DFX-NANC > FE-NANC$ , which agrees with those in case 1.

## 4.2 Performance comparison of broadband ANC systems

### 4.2.1 Case 1: White Gaussian noise

To compare the convergence speed and steady-state performance of the three computationally efficient broadband ANC systems, a stationary zero-mean white Gaussian noise with variance of 0.05 is used as the source noise signal in case 1. The reference signal is the same as the source noise signal, and the primary noise signal is obtained by passing the source noise signal through the primary path model. The duration of each independent simulation is 100 s. The length of the control filter is  $N = 256$ , the regularization constant is  $\varepsilon = 0.001$ , the number of subbands is  $G = 32$ , the decimation factor is  $D = G/2$ , the length of subband control filters is  $N_s = N/D$ , the length of subband secondary path estimates is  $\hat{M}_s = \hat{M}/D$ , the fullband weight transform rate is  $J = 2$ , the length of analysis filters is  $L = 4G$ . The step size of each system is selected experimentally to be as optimal as possible.

The conventional FX-BANC system and the NFX-BANC system serve as the references. The time waveforms of the residual noise for the five broadband ANC systems in this case are plotted in Fig. 20. Furthermore, the ANR curves and frequency spectrums of the residual noise for these systems are also compared in Fig. 21, where the ANR curves and frequency spectrums of the FX-BANC and NFX-BANC systems are overlapped. From all the results, it can be observed that all the considered broadband ANC systems are able to attenuate the broadband primary noise well, and they have the similar convergence speeds. But it can also be seen that the steady-state errors of the DS-BANC system and the MDS-BANC system are larger than those of the FX-BANC system, the NFX-BANC system and the DF-BANC system. As shown in the frequency spectrum results, the residual noise of the two subband systems including the DS-BANC system and the MDS-BANC system fluctuates largely in the frequency domain, since the noise in each frequency subband is controlled relatively independently.

### 4.2.2 Case 2: Colored noise

In this case, to further evaluate the control performance of the considered broadband ANC systems for broadband noises that have large spectral dynamic range, a colored noise obtained by filtering a zero-mean white Gaussian noise through a 10th order

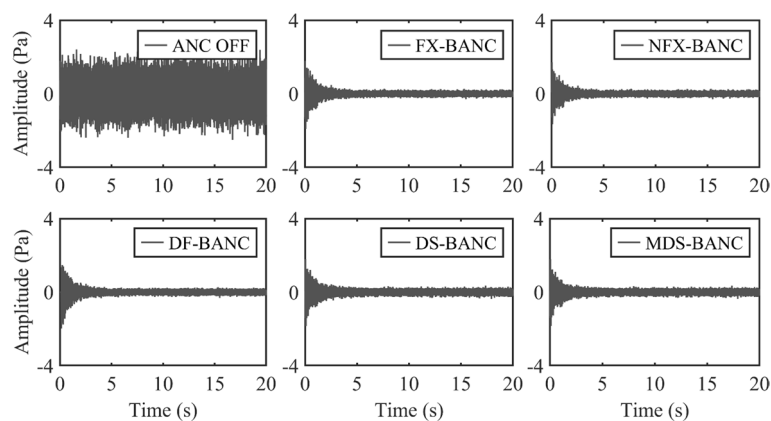


**Fig. 20** Time waveforms of the residual noise for the five broadband ANC systems in case 1



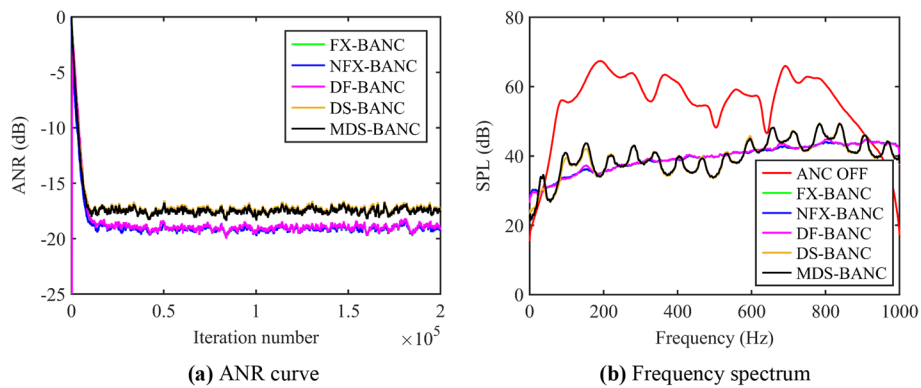


**Fig. 21** ANR curves and frequency spectrums of the residual noise for the five broadband ANC systems in case 1

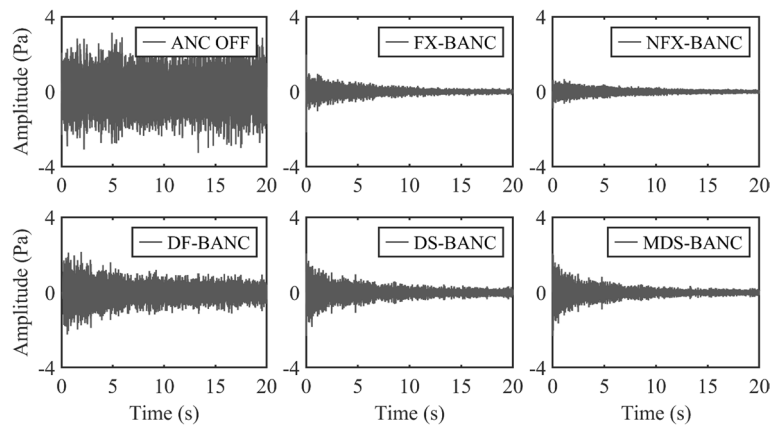


**Fig. 22** Time waveforms of the residual noise for the five broadband ANC systems in case 2

auto-regressive system [38] is used as the source noise signal. The reference signal is the same as the source noise signal, and the primary noise signal is obtained by passing the source noise signal through the primary path model. The duration of each independent simulation is 100 s. The rest of the parameter settings are the same as those in case 1.

With the synthesized colored noise signal, the performance of the five broadband ANC systems is compared. Figure 22 shows the time waveforms of the residual noise for the five broadband ANC systems in case 2. And Fig. 23 also illustrates the ANR curves and frequency spectrums of the residual noise for these systems. It is obvious from Figs. 22 and 23a that, in terms of the convergence speed and steady-state error, the NFX-BANC system performs the best, followed by the FX-BANC, MDS-BANC and DS-BANC systems, and the DF-BANC system performs the worst in this case. On the other hand, the results of Fig. 23b demonstrate that the DS-BANC system and the MDS-BANC system can eliminate the frequency components with lower amplitude levels much better than the other three broadband ANC systems. This may be because the noise signal with higher eigenvalue spread ratio can be canceled using different normalized step sizes in respective frequency subbands.

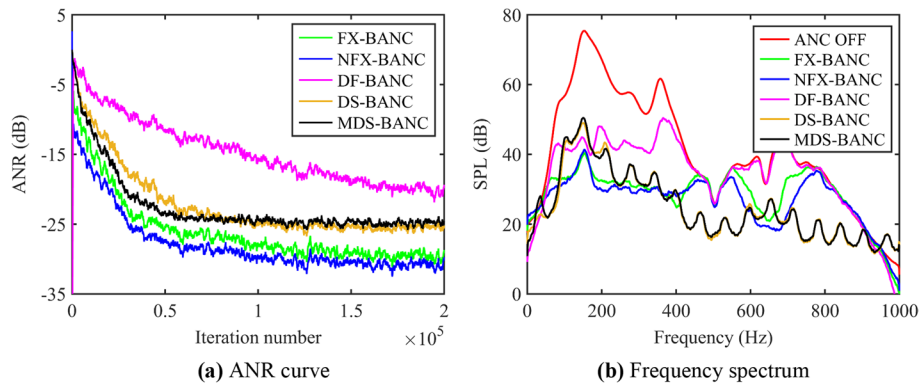


**Fig. 23** ANR curves and frequency spectrums of the residual noise for the five broadband ANC systems in case 2

### 4.3 Discussions

Based on the computational complexity analysis and numerical simulations, the relative strengths and weaknesses of the considered computational-efficient narrowband and broadband ANC systems are summarized in Tables 3 and 4, respectively. Among the narrowband ANC systems, the computational complexity of the DFX-NANC, LFE-NANC, and LFX-NANC systems are all very low, followed by the FE-NANC, CFX-NANC, and BFX-NANC systems. However, due to the inaccurate delay estimation and amplitude effect, the convergence speed and noise reduction performance of the DFX-NANC system suffer from degradation. The LFX-NANC system employs Delegà’s local secondary path estimation method, which fails to provide an accurate spectral approximation of

**Table 3** Relative strengths and weaknesses of the considered computational-efficient narrowband ANC systems

System	Computational complexity	Convergence speed	Steady-state error
DFX-NANC	Good	Fair	Fair
BFX-NANC	Fair	Good	Good
LFX-NANC	Good	Fair	Fair
FE-NANC	Fair	Bad	Bad
LFE-NANC	Good	Good	Good
CFX-NANC	Fair	Good	Good

**Table 4** Relative strengths and weaknesses of the considered computational-efficient broadband ANC systems

System	Computational complexity	White Gaussian noise		Colored noise	
		Convergence speed	Steady-state error	Convergence speed	Steady-state error
DF-BANC	Good	Good	Good	Bad	Bad
DS-BANC	Fair	Good	Fair	Fair	Fair
MDS-BANC	Fair	Good	Fair	Good	Fair

the secondary path, thus limiting the system performance. And the FE-NANC system performed the worst because of the severe delay in the convergence of the control filters.

Among the broadband ANC systems, the DF-BANC system has the lowest computational effort, followed by the MDS-BANC and DS-BANC systems. When the controlled noise is the white Gaussian noise, the noise attenuation performance of the MDS-BANC and DS-BANC systems is slightly worse than that of the DF-BANC system, but they still have good broadband attenuation effects. When the controlled noise is the colored noise with high spectral dynamics, the MDS-BANC and DS-BANC systems can effectively reduce not only the frequency components with high amplitude but also those with low amplitude due to the use of subband filtering methods. However, the convergence speed and noise attenuation performance of the DF-BANC system are poor, because it is unable to control different frequency subbands relatively independently. In fact, the optimal step sizes corresponding to different frequency subbands are different, so determining the appropriate step size combination is a very tricky problem, which we will also investigate in-depth in our future work.

Finally, in order to make all the considered ANC systems easier to understand and implement in real applications, Table 5 provides the key parameters and usage characteristics of each system.

### 5 Conclusions

In this paper, the typical narrowband and broadband ANC systems with emphasis on reducing computational complexity are reviewed. Through the computational complexity analysis and a series of numerical simulations, some valuable results are obtained as follows. For the narrowband ANC systems, the comparative results of computational superiority may be expressed as DFX-NANC > LFE-NANC > LFX-NANC > FE-NANC > CFX-NANC > BFX-NANC. The convergence speed and noise reduction performance of the LFE-NANC, CFX-NANC and BFX-NANC systems are good; whereas, those of the DFX-NANC, LFX-NANC and FE-NANC systems are unsatisfactory. For the broadband ANC systems, the comparative results of computational

**Table 5** Key parameters and usage characteristics of all the computational-efficient ANC systems

	System	Key parameters	Usage characteristics
Narrowband	DFX-NANC	$\mu_i$	Time-domain update, delay compensation method
	BFX-NANC	$\mu_i, \rho$	Time-domain update, bandpass filter method
	LFX-NANC	$\mu_i, K, \hat{M}_l$	Time-domain update, local secondary path estimation method
	FE-NANC	$\mu_i$	Time-domain update, filtered-error structure method
	LFE-NANC	$\mu_i, K, \hat{M}_l$	Time-domain update, local secondary path estimation method and filtered-error structure method
	CFX-NANC	$\mu_i$	Complex-valued update, complex signal representation method
Broadband	DF-BANC	$\mu, N, \varepsilon$	Frequency-domain update, delayless frequency-domain adaptive filtering method
	DS-BANC	$\mu, G, D, N, J, \varepsilon$	Time-domain update, delayless subband adaptive filtering method
	MDS-BANC	$\mu, G, D, N, J, \varepsilon, \hat{M}_s$	Time-domain update, modified delayless subband adaptive filtering method

superiority may be expressed as DF-BANC > MDS-BANC > DS-BANC. When the controlled noise is the white Gaussian noise, the three systems have acceptable broadband attenuation effects. However, when the controlled noise is the colored noise with high spectral dynamics, the control performance of the MDS-BANC and DS-BANC systems is much better than that of the DF-BANC system. This study may provide greater insight into typical computationally efficient ANC systems, which will be beneficial in facilitating the use of ANC technology in real-world applications.

#### Acknowledgements

The authors would like to express their sincere thanks to the editors and anonymous reviewers.

#### Author contributions

The study was designed by XL, and supervised by WC, and ZL. Data were collected by WC and CL. Data analysis was performed by XL and MS. XL and WC prepared the manuscript. All authors critically revised, read and approved the final manuscript.

#### Funding

This study was supported by National Natural Science Foundation of China (No. 52175111), the Fundamental Research Funds for the Central Universities (WUT: 2023IVA086), and Foshan Xianhu Laboratory of the Advanced Energy Science and Technology Guangdong Laboratory (No. XHD2020-003).

#### Availability of data and materials

The datasets generated or analyzed during the current study are available from the corresponding author on reasonable request.

#### Declarations

##### Ethics approval and consent to participate

Not applicable.

##### Consent for publication

Not applicable.

##### Competing interests

The authors declare no competing interests.

Received: 4 March 2023 Accepted: 28 November 2023

Published online: 09 December 2023

#### References

1. P. Lueg, Process of silencing sound oscillations. Registered patent number US 2043416 (1936)
2. C.L. Ferrari, J. Cheer, M. Mautone, Investigation of an engine order noise cancellation system in a super sports car. *Acta Acust.* **7**, 1 (2023)
3. S. Kim, M.E. Altinsoy, Comprehensive active control of booming noise inside a vehicle caused by the engine and the driveline. *IEEE Access* **10**, 49725–49737 (2022)
4. W. Jung, S.J. Elliott, J. Cheer, Local active control of road noise inside a vehicle. *Mech. Syst. Signal Process.* **121**, 144–157 (2019)
5. J. Cheer, S.J. Elliott, Active noise control of a diesel generator in a luxury yacht. *Appl. Acoust.* **105**, 209–214 (2016)
6. D. Sachau, S. Jukkert, N. Hövelmann, Development and experimental verification of a robust active noise control system for a diesel engine in submarines. *J. Sound Vib.* **375**, 1–18 (2016)
7. Q. Yu, E. Cao, Active control for marine engine room noise using an FXLMS algorithm. *Sci. Program.* **2022**, 1–11 (2022)
8. J. Buck, D. Sachau, Active headrests with selective delayless subband adaptive filters in an aircraft cabin. *Mech. Syst. Signal Process.* **148**, 107164 (2021)
9. C.Y. Chang, C.T. Chuang, S.M. Kuo, C.H. Lin, Multi-functional active noise control system on headrest of airplane seat. *Mech. Syst. Signal Process.* **167**, 108552 (2022)
10. I. Dimino, C. Colangeli, J. Cuenca, P. Vitiello, M. Barbarino, Active noise control for aircraft cabin seats. *Appl. Sci.* **12**(11), 5610 (2022)
11. S.M. Kuo, D.R. Morgan, *Active Noise Control Systems: Algorithms and DSP Implementations* (Wiley, New York, 1996)
12. S.M. Kuo, D.R. Morgan, Active noise control: a tutorial review. *Proc. IEEE* **87**(6), 943–973 (1999)
13. C. Sun, Y. Liu, Z. Bo, S. Jiang, A new online secondary path modeling method with an auxiliary noise power scheduling strategy for narrowband active noise control systems. *Appl. Sci.* **7**, 1236 (2017)
14. J. Liu, X. Chen, L. Yang, J. Gao, X. Zhang, Analysis and compensation of reference frequency mismatch in multiple-frequency feedforward active noise and vibration control system. *J. Sound Vib.* **409**, 145–164 (2017)
15. R. Han, M. Wu, F. Liu, H. Sun, J. Yang, A narrowband active noise control system with a frequency estimator based on Bayesian inference. *J. Sound Vib.* **455**, 299–311 (2019)

16. Y. Ma, Y. Xiao, L. Ma, K. Khorasani, Statistical analysis of narrowband active noise control using a simplified variable step-size FXLMS algorithm. *Signal Process.* **183**, 108012 (2021)
17. N.J. Bershad, J.C.M. Bermudez, A switched variable step size NLMS adaptive filter. *Digit. Signal Process.* **101**, 102730 (2020)
18. H. Meng, S. Chen, Particle swarm optimization based novel adaptive step-size FxLMS algorithm with reference signal smoothing processor for feedforward active noise control systems. *Appl. Acoust.* **174**, 107796 (2021)
19. Y. Han, M. Wang, M. Liu, An improved variable tap-length algorithm with adaptive parameters. *Digit. Signal Process.* **74**, 111–118 (2018)
20. S.H. Pauline, D. Samiappan, R. Kumar, A. Anand, A. Kar, Variable tap-length non-parametric variable step-size NLMS adaptive filtering algorithm for acoustic echo cancellation. *Appl. Acoust.* **159**, 107074 (2020)
21. A. Kar, A. Anand, M.N.S. Swamy, Automatic tap-length adjustment of adaptive filter for feedback attenuation in hearing aids. *Appl. Acoust.* **158**, 107043 (2020)
22. J.K. Thomas, S.P. Lovstedt, J.D. Blotter, S.D. Sommerfeldt, Eigenvalue equalization filtered-x algorithm for the multi-channel active noise control of stationary and nonstationary signals. *J. Acoust. Soc. Am.* **123**(6), 4238–4249 (2008)
23. M.T. Akhtar, W. Mitsuhashi, Improving robustness of filtered-x least mean p-power algorithm for active attenuation of standard symmetric- $\alpha$ -stable impulsive noise. *Appl. Acoust.* **72**(9), 688–694 (2011)
24. G. Sun, M. Li, T.C. Lim, A family of threshold based robust adaptive algorithms for active impulsive noise control. *Appl. Acoust.* **97**, 30–36 (2015)
25. L. Wu, H. He, X. Qiu, An active impulsive noise control algorithm with logarithmic transformation. *IEEE Trans. Audio Speech Lang. Process.* **19**(4), 1041–1044 (2011)
26. M.T. Akhtar, A time-varying normalized step-size based generalized fractional moment adaptive algorithm and its application to ANC of impulsive sources. *Appl. Acoust.* **155**, 240–249 (2019)
27. E.J. Ziegler, Selective active cancellation system for repetitive phenomena. Registered patent number US 4878188 A, 1989.
28. B. Simon, N. Fabbiane, T. Nemitz et al., In-flight active wave cancelation with delayed-x-LMS control algorithm in a laminar boundary layer. *Exp. Fluids* **57**, 160 (2016)
29. Y. Xiao, A new efficient narrowband active noise control system and its performance analysis. *IEEE Trans. Audio Speech Lang. Process.* **19**(7), 1865–1874 (2011)
30. R. Delegà, G. Bernasconi, L. Piroddi, A novel cost-effective parallel narrowband ANC system with local secondary-path estimation. *J. Sound Vib.* **401**, 311–325 (2017)
31. C. Chang, S.M. Kuo, C. Huang, Secondary path modeling for narrowband active noise control systems. *Appl. Acoust.* **131**, 154–164 (2018)
32. W. Chen, C. Lu, H. Williams, Z. Liu, Y. Sun, Development and experimental verification of a new computationally efficient parallel narrowband active noise control system. *Appl. Acoust.* **187**, 108510 (2022)
33. W. Chen, C. Lu, Z. Liu, H. Williams, L. Xie, A computationally efficient active sound quality control algorithm using local secondary-path estimation for vehicle interior noise. *Mech. Syst. Signal Process.* **168**, 108698 (2022)
34. W. Zhu, L. Luo, A. Xie, J. Sun, A novel FELMS-based narrowband active noise control system and its convergence analysis. *Appl. Acoust.* **156**, 229–245 (2019)
35. D.C. Le, J. Zhang, D. Li, S. Zhang, A generalized exponential functional link artificial neural networks filter with channel-reduced diagonal structure for nonlinear active noise control. *Appl. Acoust.* **139**, 174–181 (2018)
36. L. Luo, Z. Bai, W. Zhu, J. Sun, Improved functional link artificial neural network filters for nonlinear active noise control. *Appl. Acoust.* **135**, 111–123 (2018)
37. H. Jeon, T. Chang, S.M. Kuo, Analysis of frequency mismatch in narrowband active noise control. *IEEE Trans. Audio Speech Lang. process.* **18**(6), 1632–1642 (2010)
38. S.M. Kuo, R.K. Yenduri, A. Gupta, Frequency-domain delayless active sound quality control algorithm. *J. Sound Vib.* **318**(4), 715–724 (2008)
39. J. Duan, M. Li, T.C. Lim, A computational-efficient active sound tuning system for steady-state and transient vehicle powertrain response. *Int. J. Veh. Noise Vib.* **10**(1–2), 77–92 (2014)
40. L. Yin, Z. Zhang, M. Wu, Z. Wang, C. Ma, S. Zhou, J. Yang, Adaptive parallel filter method for active cancellation of road noise inside vehicles. *Mech. Syst. Signal Process.* **193**, 110274 (2023)
41. L. Wang, K. Chen, J. Xu, A subband adaptive filtering for distributed active noise control systems. *IEEE Trans. Electr. Electron. Eng.* **16**(3), 436–444 (2021)
42. Z. Zhou, S. Chen, H. Li, Y. Cai, Delayless partial subband update algorithm for feed-forward active road noise control system in pure electric vehicles. *Mech. Syst. Signal Process.* **196**, 110328 (2023)
43. G. Long, T.C. Lim, A new robust delayless subband adaptive filtering algorithm with variable step sizes for active control of broadband noise. *Appl. Acoust.* **176**, 107858 (2021)
44. D. Shi, B. Lam, W. Gan, S. Wen, Block coordinate descent based algorithm for computational complexity reduction in multichannel active noise control system. *Mech. Syst. Signal Process.* **151**, 107346 (2021)
45. K. Iwai, S. Kinoshita, Y. Kajikawa, Multichannel feedforward active noise control system combined with noise source separation by microphone arrays. *J. Sound Vib.* **453**, 151–173 (2019)
46. L. Yang, W. Gao, J. Yang, B. Zhao, L. Liu, A novel active control strategy with decentralized decoupling and wavelet packet transformation: design and verification. *Appl. Sci.* **11**(8), 3554 (2021)
47. S. Pradhan, G. Zhang, X. Qiu, A time domain decentralized algorithm for two channel active noise control. *J. Acoust. Soc. Am.* **147**(6), 3808–3813 (2020)
48. M. Kamaldar, J.B. Hoagg, Centralized and decentralized adaptive harmonic control for sinusoidal disturbance rejection. *Control. Eng. Pract.* **112**, 104814 (2021)
49. Y. Dong, J. Chen, W. Zhang, Wave-domain active noise control over distributed networks of multi-channel nodes. *Signal Process.* **184**, 108050 (2021)
50. J. Chen, M. Wu, C. Gong, X. Wang, J. Yang, Steady-state performance analysis of the distributed FxLMS algorithm for narrowband ANC system with frequency mismatch. *IEEE Signal Process. Lett.* **29**, 1167–1171 (2022)

51. Y. Chu, M. Wu, H. Sun, J. Yang, M. Chen, Some practical acoustic design and typical control strategies for multichannel active noise control. *Appl. Sci.* **12**(4), 2244 (2022)
52. C. Antoñanzas, M. Ferrer, M. de Diego, A. Gonzalez, Remote microphone technique for active noise control over distributed networks. *IEEE Trans. Audio Speech Lang. Process.* **31**, 1522–1535 (2023)
53. L. Lu, K. Yin, R.C. de Lamare et al., A survey on active noise control in the past decade-Part I: linear systems. *Signal Process.* **183**, 108039 (2021)
54. J. Jiang, Y. Li, Review of active noise control techniques with emphasis on sound quality enhancement. *Appl. Acoust.* **136**, 139–148 (2018)
55. F. Yang, Y. Cao, M. Wu, F. Albu, J. Yang, Frequency-domain filtered-x LMS algorithms for active noise control: a review and new insights. *Appl. Sci.* **8**(11), 2313 (2018)
56. S.M. Chen, F.H. Gu, C. Liang et al., Review on active noise control technology for alpha-stable distribution impulsive noise. *Circuits Syst. Signal Process.* **41**(2), 956–993 (2022)
57. A. Nehorai, A minimal parameter adaptive notch filter with constrained poles and zeros. *IEEE Trans. Acoust. Speech Signal Process.* **33**(4), 983–996 (1985)
58. S. Elliott, *Signal processing for active control* (Academic Press, London, 2001)
59. S. Zhang, Y.S. Wang, H. Guo et al., A normalized frequency-domain block filtered-x LMS algorithm for active vehicle interior noise control. *Mech. Syst. Signal Process.* **120**, 150–165 (2019)
60. P. Song, H. Zhao, Filtered-x generalized mixed norm (FXGMN) algorithm for active noise control. *Mech. Syst. Signal Process.* **107**, 93–104 (2018)

### Publisher's Note

Springer Nature remains neutral with regard to jurisdictional claims in published maps and institutional affiliations.

**Submit your manuscript to a SpringerOpen<sup>®</sup> journal and benefit from:**

- ▶ Convenient online submission
- ▶ Rigorous peer review
- ▶ Open access: articles freely available online
- ▶ High visibility within the field
- ▶ Retaining the copyright to your article

---

Submit your next manuscript at ▶ [springeropen.com](https://www.springeropen.com)

---